ATMOSPHERIC ENVIRONMENT: X 26 (2025) 100329

Contents lists available at ScienceDirect

Atmospheric Environment: X

journal homepage: www.journals.elsevier.com/atmospheric-environment-x

Enhanced thermal performance and hydrochloric acid gas (HCl) emission mitigation in ammonium perchlorate (AP)-Based solid propellants with potassium permanganate ($KMnO_4$)/AP dual oxidisers

Izzat Najmi Yaacob [a,b], Ezanee Gires [a,b], Adi Azrif Basri [a,b], Kamarul Arifin Ahmad [a,b], Kamsani Kamal [d], Nor Afizah Salleh [d], Suraya Shahedi [d], Fikri Rasih [d], Zakwan Azizi [e], Sharul Sham Dol [f], Norkhairunnisa Mazlan [a,b,c,*]

[a] Department of Aerospace Engineering, Faculty of Engineering, Universiti Putra Malaysia, UPM Serdang, 43400, Selangor, Malaysia
[b] Aerospace Malaysia Research Center (AMRC), Universiti Putra Malaysia, UPM Serdang, 43400, Selangor, Malaysia
[c] Institute of Nanoscience and Nanotechnology (ION2), Universiti Putra Malaysia, UPM Serdang, 43400, Selangor, Malaysia
[d] Science & Technology Research Institute for Defence (STRIDE), Government of Malaysia, 43000, Kajang, Selangor, Malaysia
[e] School of Mechanical Engineering, College of Engineering, Universiti Teknologi MARA, 40450, Shah Alam, Selangor, Malaysia
[f] Mechanical and Industrial Engineering Department, Abu Dhabi University, PO Box 59911, Abu Dhabi, United Arab Emirates

ARTICLE INFO

Keywords:
Solid propellant
Ammonium perchlorate
Environmentally friendly
Hydrochloric gas
Dual oxidiser

ABSTRACT

The conventional propellant used in rocket boosters and tactical missiles commonly utilises ammonium perchlorate (AP). However, the release of harmful chloride fumes resulting from the combustion of AP during rocket launches contributes to a 1 % increase in air pollution. Generally, the perchlorate-based propellants contribute to pollution by hydrochloric acid (HCl), which can contaminate launch sites and potentially deplete the ozone layer. Several techniques have been employed to convert standard AP-based composite solid propellant (CSP) into green propellant. This study designed a minimum chlorine content propellant containing potassium permanganate, $KMnO_4$/AP as a dual oxidiser and examined its properties in CSP formulation. This novel $KMnO_4$/AP was characterised in terms of morphological structure, elemental analysis, and thermal decomposition properties by using scanning electron microscope (SEM), energy dispersive X-ray analysis (EDX), and differential scanning calorimetry (DSC) and thermogravimetry analysis (TGA), respectively. Additionally, heat of combustion analysis was examined through bomb calorimetry. The chlorine content investigations were experimentally carried out, and the results were compared with conventional AP-based CSP using gas bubbling and Mohr's titration method. From thermal decomposition analysis, sample $KMnO_4$/AP (40:60) shifted high temperature decomposition (HTD) of AP to a lowest temperature of 331.32 °C with the highest heat release of 3721.2 J/g. Besides, sample $KMnO_4$/AP (80:20) shows the highest reduction of chlorine concentration content with a reduction percentage of 58.25 %. Besides, $KMnO_4$/AP (40:60) sample resulted in the highest value of heat of combustion with a value of 1254.01 cal/g. This study contributes to the development of environmentally friendly and sustainable oxidisers for solid rocket propellant applications.

1. Introduction

Composite solid propellant (CSP) has been extensively used in space exploration and defence technologies for decades (Adeniyi et al., 2021). They are specifically engineered to enhance the speed of projectiles, rockets, missiles, space launchers, or aeroplane ejection seats by generating propulsive force. Due to their favourable characteristics such as reasonable cost, strong mechanical and combustion properties, simplicity, reliability, and ease of processing and storage, the most developed propellant composition consists of ammonium perchlorate (AP) as the oxidiser, hydroxyl-terminated polybutadiene (HTPB) as the binder, and aluminium (Al) as the fuel (Pang et al., 2021; Okniński et al., 2020). CSP using ammonium perchlorate (AP) as an oxidiser has a detrimental effect on the atmosphere as it releases hydrochloric acid (HCl) as a significant component of its exhaust. Trache et al. (2017a) stated that thermodynamic calculations indicate that a typical

* Corresponding author. Department of Aerospace Engineering, Faculty of Engineering, Universiti Putra Malaysia, UPM Serdang, 43400, Selangor, Malaysia.
E-mail address: norkhairunnisa@upm.edu.my (N. Mazlan).

https://doi.org/10.1016/j.aeaoa.2025.100329
Received 6 March 2025; Received in revised form 1 May 2025; Accepted 9 May 2025
Available online 10 May 2025

composition utilized in Ariane V boosters, consisting of 68 % ammonium perchlorate (AP), 18 % aluminium (Al), and 14 % elastomeric binder, results in the production of around 21 % hydrochloric acid. In addition, the propellant used in the Space Shuttle releases a significant amount of hydrogen chloride (HCl) at a concentration of 21 % (DeLuca et al., 2017). This emission contaminates the stratosphere and affects terrestrial and aquatic ecosystems. In addition, the launch of six Titan-class spacecraft can result in ozone depletion and a significant rise in stratospheric acidic rain (Maggi et al., 2023a). Another concern in military applications is the formation of nucleation sites for aerosolized water products by HCl gas. This leads to secondary smoke in the exhaust plume, which can be visible or detected by radar (Abdelhafiz et al., 2021; Bogusz and Magnuszewska, 2019). Consequently, developing the next generation of solid propellants must consider environmental factors while ensuring high performance.

For over five decades, AP-based CSP has been used as a solid propellant system. The inorganic compound AP, which has the chemical formula NH_4ClO_4, is a highly potent oxidiser in solid propulsion systems. This white crystalline substance easily dissolves in water and is produced through the reaction between ammonia and perchloric acid. Additionally, Maggi et al. (2023b) claimed that AP is also considered a superior oxidiser compared to other oxidisers, attributing its exceptional ballistic performance and mechanical properties. Due to its numerous benefits, it has a prominent role as the primary oxidiser in CSP and is primarily utilized in missiles and boosters (Kopacz et al., 2022). When AP is employed as an oxidiser in a solid rocket motor, it undergoes a chemical reaction with a fuel source such as aluminium powder or a polymer binder to generate gases of elevated temperature (Kopacz et al., 2022; DeLuca et al., 2018). These gases are responsible for generating the necessary thrust for propulsion. Upon exposure to elevated temperatures, AP undergoes a decomposition process, releasing gases and forming solid residues. The decomposition reaction may be expressed as shown in the study conducted by DeLuca et al. (Schuch and Fisch, 2019) as follows:

$$NH_4ClO_4 \rightarrow H_2O + N_2 + 4HCl + 3/2O_2 \quad (1)$$

The decomposition process of AP creates water (H_2O), nitrogen gas (N_2), hydrogen chloride gas (HCl), and oxygen gas (O_2). This process is accompanied by a highly exothermic decomposition reaction that emits a significant amount of heat (Gańczyk-Specjalska et al., 2021). This characteristic is particularly valuable for its use as an oxidiser in rocket propellants, where the gases produced contribute to thrust generation. To understand the thermal decomposition of AP, researchers commonly employ thermogravimetric analysis (TGA) and differential scanning calorimetry (DSC) techniques. These methods allow for the precise temperature at which AP decomposes (DeLuca et al., 2018; Schuch and Fisch, 2019; Gańczyk-Specjalska et al., 2021; Chalghoum et al., 2020). Xu et al. (2021) claimed that this thermal decomposition study is a very important parameter in the study of CSP as AP is the primary ingredient in the formulation of propellant hence its decomposition plays a crucial part in the whole combustion process of the propellant.

Three approaches have been examined for reducing HCl in the combustion plume of CSP (Trache et al., 2018): (i) using propellants with reduced chlorine content (Terry et al., 2016); (ii) neutralising HCl acid within the combustion plume (Chalghoum et al., 2020; Xu et al., 2021; Trache et al., 2018; Terry et al., 2016); and (iii) removal of chlorine ions using alkali metals (Vellaisamy and Biswas, 2020). While these methods have effectively reduced HCl levels in the AP-based CSP combustion plume, they have also compromised optimal performance metrics, such as burn rate, specific impulse, and calorific combustion properties, particularly at lower altitudes (Xiong et al., 2023). Despite previous efforts to remove the chlorine ion, which yielded less than ideal results, exploring new ways to incorporate alkali metals may lead to enhance performance. The initial technique extensively investigated involves replacing AP with other energetic oxidisers. Recent evaluations by Trache et al. (2018) have identified potential substitutes for AP, yet no chlorine-free solid oxidisers currently match or surpass AP in performance. Strategies such as reducing, eliminating, or removing HCl during combustion have effectively addressed the environmental impact of AP-based CSP. Klapötke et al. (2009) have stated that adding $NaNO_3$ enables the conversion of gaseous chlorine into NaCl. Doll and Lund (1992a) demonstrated that the addition of magnesium (Mg) produces a low-acid propellant, which signifies a significant advancement in the field of ecologically friendly solid propulsion technology. D'Andrea et al. (D'Andrea et al., 2000) provided a comprehensive set of experimental studies in this regard. Nevertheless, these techniques have the potential to adversely impact safety requirements or diminish performance. Therefore, it is necessary to create and include additional substances or components into propellant formulations that demonstrate exceptional performance and produce ecologically friendly combustion by-products. When selecting solid propellants, it is crucial to consider theoretical energetic performance and factors such as burn rate, mechanical behaviour, smokeless considerations, safety and vulnerability, ageing properties, and production cost, ensuring a comprehensive evaluation of their characteristics (de Flon et al., 2011; He et al., 2019).

Potassium permanganate ($KMnO_4$) is an exceptionally potent oxidising agent that finds extensive application in both laboratory and industrial applications. The permanganate ion (MnO_4^-) exhibits significant oxidising characteristics due to the high oxidation state of manganese (+7) (Polis et al., 2022). $KMnO_4$ is sometimes used in solid fuel applications, particularly in pyrotechnics or as an ignition source during emergencies, due to its strong oxidising properties. When incorporated into solid fuel formulations, it can serve as an oxidiser, improving combustion (Zhang et al., 2024; Shi and Feng, 2024; Najser et al., 2022). In some solid fuel formulations, potassium permanganate may also be combined with a fuel source and other additives to create a composition that releases heat and gas when ignited. This can be useful in applications such as emergency fire starters, signal flares, or other pyrotechnic devices (Fahd et al., 2021; Sun et al., 2022). Despite its widespread use, no studies have reported the application of $KMnO_4$ in neither sugar-based nor AP-based solid rocket propellants. Typically, CSP utilises AP or ammonium nitrate (AN) as the oxidiser, with the fuel being either powdered metal or a hydrocarbon-based substance (Sun et al., 2022). Given its strong oxidising characteristics and the production of non-toxic gases upon combustion, it is proposed that novel $KMnO_4$/AP dual oxidiser has the potential to be as main oxidiser in AP-based CSP formulation. This paper will explore the fabrication method, characterisation of CSP with KMnO4/AP as a novel dual oxidiser and compare the reduction in chlorine concentration to that of conventional formulations.

2. Experimental methodology

2.1. Materials and apparatus

All the chemicals used in this study were supplied by the Science & Technology Research Institute for Defense (STRIDE) and Universiti Putra Malaysia (UPM). The composition of the CSP includes several components, with the oxidiser being the predominant component, accounting for 65–80 % of the propellant's total weight. Other components include a fuel binder, plasticizer, curing agent, and crosslinking agent. Ammonium perchlorate (AP), which contributes up 70 wt% of the sample's weight, was the chose oxidiser for this research. The hydroxyl-terminated polybutadiene (HTPB) binder system contributing 13.5 wt% to the whole composition formulation. Aluminium as fuel, dioctyl adipate as a plasticizer, and toluene diisocyanate as a curing agent were also used to complete the CSP sample composition, with each of them contributing 12 %, 3.5 %, and 1 %, respectively. $KMnO_4$ supplied by R&M Chemicals with purity of 99 % is used to synthesis $KMnO_4$/AP dual oxidiser.

2.2. Potassium permanganate ($KMnO_4$)/ammonium perchlorate (AP) dual oxidiser synthesis

$KMnO_4$ crystals were ground and blended with AP powder for 30 min using agate mortar containing 1 mL of ethanol to produce a 20:80 ratio, resulting in a total weight of 3g for the $KMnO_4$/AP mixture, as described by Chen et al. (2018), which the authors synthesised the manganese oxide (MnO_4) with AP. This process aimed to ensure the homogeneous dispersion of the samples. The mixture was then vacuum filtered to separate the $KMnO_4$/AP blend. Next, the $KMnO_4$/AP mixture was dried at 70 °C for 1 h and prepared for characterisation. The samples were stored in a desiccator filled with silica gel to prevent the absorption, which could affect the materials' properties (Garino et al., 2021). Samples of $KMnO_4$/AP were prepared in weight ratios of 20:80, 40:60, 60:40, and 80:20, alongside pure AP and pure $KMnO_4$ samples. The specific quantities for each ratio quantity are shown in Table 1.

2.3. Composite solid propellant (CSP) sample preparation

The fabrication process of CSP samples is illustrated in Fig. 1. Initially, all the chemicals and powder were weighed and sieved, as illustrated in Fig. 1 (a) and 1 (b), respectively. First, dioctyl adipate (DOA) plasticizer was added to the polymer binder HTPB, and the mixture was stirred for 5 min to get a preliminary mix. Secondly, aluminium (Al) powder was incrementally added to the premix in the kneading mixer maintained at 45 °C, as shown in Fig. 1(c). Each batch was mixed for 5 min. Next, the first increment of $KMnO_4$/AP oxidiser was added to the mixture and stirred for 5 min. Then the second and third increments of $KMnO_4$/AP were then added, each stirred for an additional 25 min to ensure uniform distribution, given the oxidiser's pivotal role in the CSP formulation. Next, toluene diisocyanate as a curing agent was incrementally added while mixing continued for 40 min. The resulting propellant slurry was then casted into the sample mould and cured in an oven at 60 °C oven for 5 days, as shown in Fig. 1 (d) and 1 (e). The prepared CSP samples in Fig. 1 (f), were then ready for the evaluation of their characteristics and performance. The specifications of the sample will be described in each of the experimental test subsections. This procedure was repeated to produce samples of $KMnO_4$/AP in various $KMnO_4$ to AP ratios as formulated in Table 2.

2.4. Characterisation of composite solid propellant (CSP) samples

Scanning Electron Microscopy (SEM) was used to analyse the CSP samples' internal morphology, including internal structure, particle orientation and its distributions. SEM imaging was conducted using a FEI Model NOVA NANOSEM 230, for structural characterisation at an acceleration voltage of 120 kV. Besides, elemental analysis of the samples was analysed using Energy Dispersive X-ray (EDX) analysis using Oxford Instruments (Max 20). Through EDX analysis, the elements existed in the propellant sample's formulation were identified. The catalytic effects of $KMnO_4$ on the thermal decomposition of AP were studied and analysed by using thermogravimetric analysis (TGA) and differential scanning calorimetry (DSC), employing a Mettler Toledo (Model TGA-DSC HT 3). Specimens, both in powder and solid forms, and weighing approximately 20 mg, were placed in crucibles. The samples were held at 25 °C for 1 min before being heated to 1000 °C at a rate of 20 K/min under a nitrogen gas flow rate of 50 mL/min. The results from all samples were plotted into a single TGA and DSC graph for comparison against the pure AP decomposition curve as a reference.

Table 1
Sample size and the chemical composition of $KMnO_4$/AP dual oxidiser.

Label	AP	$KMnO_4$	$KMnO_4$/AP (20:80)	$KMnO_4$/AP (40:60)	$KMnO_4$/AP (60:40)	$KMnO_4$/AP (80:20)
$KMnO_4$ to AP ratio	–	–	20:80	40:60	60:40	80:20
AP	350 g	–	280 g	210 g	140 g	70 g
$KMnO_4$	–	350 g	70 g	140 g	240 g	280 g
Total weight	350 g	350 g	350 g	350 g	350 g	350 g

2.5. Heat of combustion study

The investigation into $KMnO_4$ efficacy in converting the chemical energy of AP-based CSP into thermal energy during combustion was conducted through the heat of combustion analysis. Bomb calorimetry provided calorimetric values, specifically using Parr 6100 instruments, from Germany. The densities of the propellant compositions were determined using a Mettler density kit, which indicated a density of 1.432 g/cm^3, and a heat of formation of 565.8 kJ mol. CSP samples were affixed to the iron wire before being placed into the bomb calorimetric chamber. For ignition, the propellant sample was connected to a nichrome wire linked to the. To minimise heat exchange with the environment and to capture the heat released during the reaction, a water bath jacket surrounded the bomb calorimetry. The observed heat of combustion values were tabulated. Besides, the combustion efficiency of each of the samples was calculated using the following equation using the theoretical value:

$$Combustion\ efficiency\ (\%) = \frac{Heat\ output}{Heat\ input}\ x\ 100 \quad (2)$$

Where heat output is the actual heat released during combustion, and heat input is the theoretical maximum heat that could be released during combustion based on the heat of combustion data. Heat input is taken from (Rao et al., 2016) as 1251 cal/g. The heat of combustion value can be determined using follows equation, and all the parameters in the formula are calculated and can be integrated straight away from the machine:

$$Q = \frac{C\Delta T - q1}{m} \quad (3)$$

Where Q is heat of combustion (J/g); C is thermal capacity of the calorimeter (J/K); ΔT is the measured temperature increase during combustion (°C); $q1$ is heat of explosion of initiation wire (J); m is the mass of sample (g).

2.6. Hydrochloric concentration reduction test setup

Using gas bubbling equipment and Mohr's titration method, the concentration of hydrochloric acid gases (HCl) as combustion by-products from each combusted sample was detected. This method was employed by Vellaisamy et al. (Vellaisamy and Biswas, 2020) which the investigation into the effects of metal additives on HCl concentrations as a combustion by-product of AP-based CSP. Besides, Mohr's method is a widely recognised analytical technique for determining the concentration of chloride ions in a solution, adhering to the standard of water quality determination of chloride (ISO 9297:1989). A sample of CSP measuring 6 mm × 6 mm x 100 mm was cut, and a 5 cm of visco fuse wire was attached to the propellant sample, as shown in Fig. 2(a). The CSP sample was put in a test tube with a side arm and sealed with a stopper at the top. The visco fuse wire was ignited using fire when the setup was ready. Fig. 2 (b) shows the CSP samples used in this experimental work.

2.6.1. Gas bubbling method

The rubber tube was connected by attaching the test tube's side arm to the nozzle of a 2 L wash bottle. A wash bottle containing 0.8 L of distilled water was utilized to channel the exhaust gases through the water by the process of bubbling. A glass tube with a diameter of

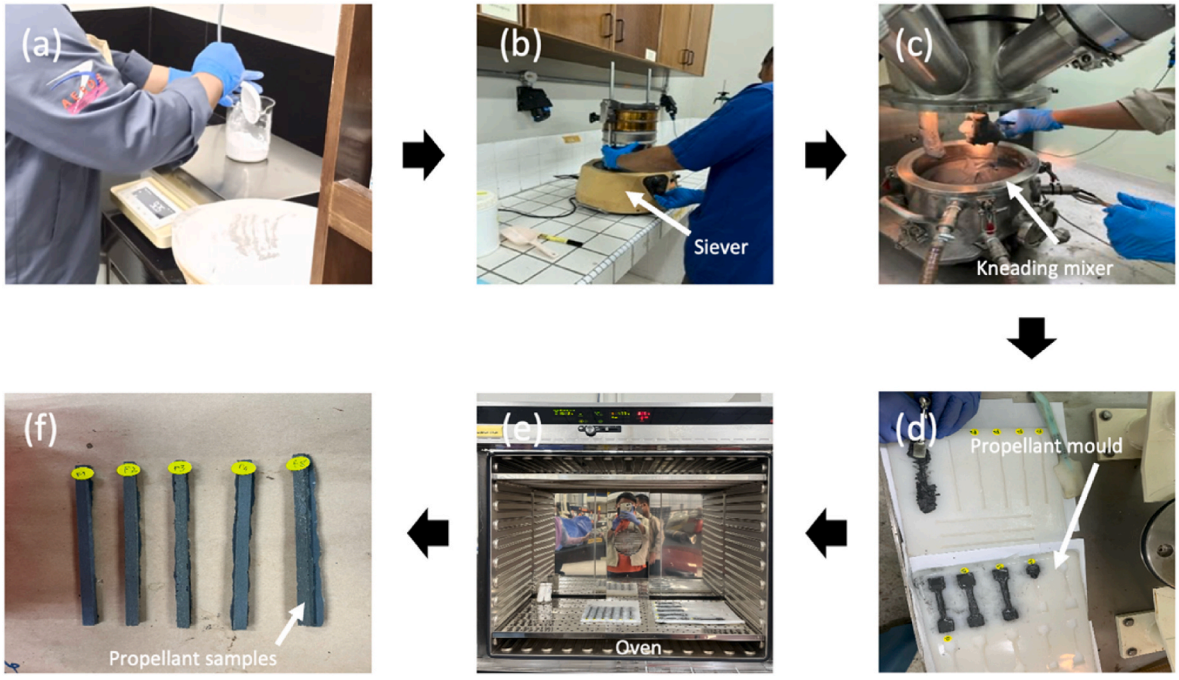

Fig. 1. Overall fabrication process of composite solid propellant (CSP) samples.

Table 2
Composition of composite solid propellant (CSP) sample.

Sample	Oxidiser ($KMnO_4$: AP) (%)	Fuel (%)	Binder (%)	Plasticizer (%)	Curing agent (%)
AP CSP	(0:100) 70	12	13.5	3.5	1
$KMnO_4$/AP (20:40) CSP	(20:80) 70	12	13.5	3.5	1
$KMnO_4$/AP (40:60) CSP	(40:60) 70	12	13.5	3.5	1
$KMnO_4$/AP (60:40) CSP	(60:40) 70	12	13.5	3.5	1
$KMnO_4$/AP (80:20) CSP	(80:20) 70	12	13.5	3.5	1

Fig. 2. (a) CSP sample with visco fuse wire (b) 6 mm × 6 mm x 100 mm propellant sample.

approximately 0.3 m was immersed in distilled water to allow the exhaust gas to create bubbles. The exhaust gas collection tests were conducted in an inert environment and at ambient pressure. Following the release of exhaust gases, the water sample is subjected to titration to determine the chloride concentration of the exhaust gases. Fig. 3 illustrates the gas bubbling setup used in this research work.

2.6.2. *Mohr's titration method*

The procedure used for determining the chloride concentration in the water sample is detailed as follows, with Fig. 4 illustrating the setup

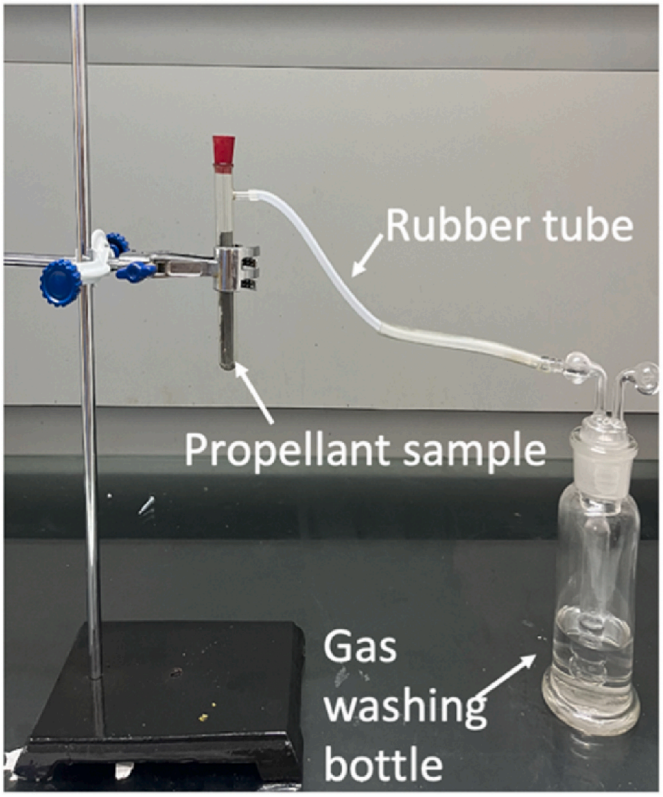

Fig. 3. Gas bubbling method setup.

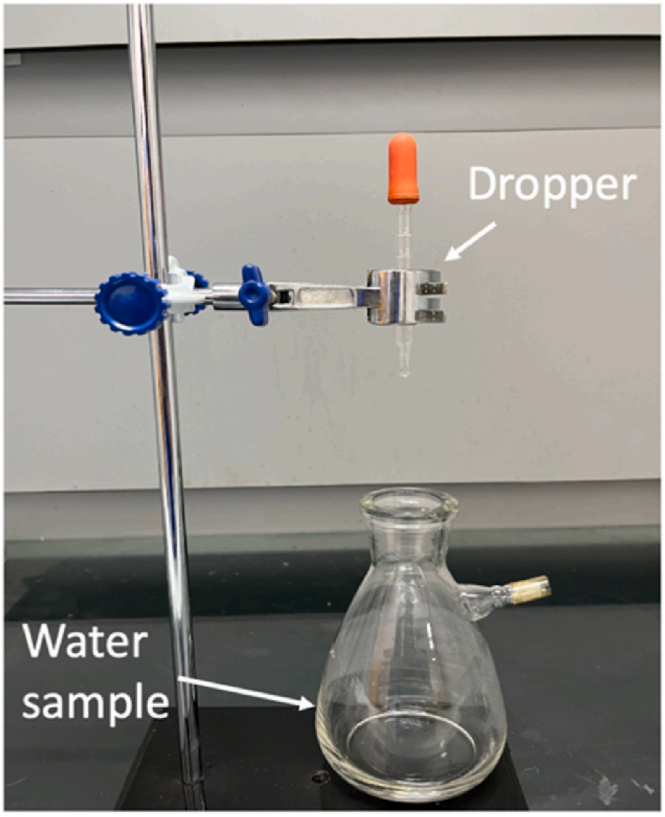

Fig. 4. Mohr's titration method setup.

for Mohr's titration method. Initially, a dropper pipette was employed to transfer 5 mL of 0.1 M silver nitrate ($AgNO_3$) solution into a glass funnel. Next, a 10 mL water sample, depicted in Fig. 5(a) was poured into a conical flask, to which 2–3 drops of 0.25 M potassium chromate (K_2CrO_4) solution were added. Next, the water sample underwent titration with silver nitrate solution by gradually adding the silver nitrate solution from the dropper pipette. This addition leads to a change in the colour of the K_2CrO_4 to a yellowish milky colour as depicted in Fig. 5 (b).

The titration concluded when a reddish-brown precipitate appeared, as shown in Fig. 5 (c), at which point the volume of the silver nitrate solution dispensed from the dropper pipette was recorded. This procedure was repeated three times to ensure accuracy, allowing for the calculation of an average result.

2.6.3. Chlorine concentration calculation analysis

Based on (Hamim et al., 2023) the first calculation is to determine the chloride ion using the formula:

$$M1V1 = M2V2 \quad (4)$$

Where $M1$ is molarity of $AgNO_3$, $V1$ is the volume used in dropper pipette, $M2$ is the molarity of water sample, and $V2$ is the volume of the water sample. Chloride content in the water sample is determined by using the following formula:

$$\text{Chlorine content (ppm)} : \textit{molarity of water samples}\ (M2)\ x\ 35.5\ x\ 1000 \quad (5)$$

The molar mass of HCl is 35.5 g/mol (Doll and Lund, 1992b). The procedure described earlier is executed for every water sample containing dissolved propellant exhaust gases to determine the chloride concentration of each propellant sample. Each sample was subjected to three titrations, and the chloride concentration was calculated for each titration to compute the average value. The result data on the chloride content in ppm of all the samples has been tabulated.

3. Experimental results and analysis

3.1. $KMnO_4$/AP composite solid propellant (CSP) characterizations

3.1.1. Physical characteristics of composite solid propellant (CSP)

The CSP samples were produced using the previously mentioned procedure, and upon curing, noticeable variations were observed among the samples. Fig. 6 depicts the physical condition of all samples following the curing process.

As seen in Fig. 6 (a), the AP CSP sample had a typical CSP color, which is grey with sporadic white particles. The grey color is a result of the presence of aluminium particles, whereas the little white particle is referred to as AP. When $KMnO_4$ was introduced, the CSP exhibited a darker appearance, and the surface of the samples became more rougher, as seen in Fig. 6 (b). As the ratio of $KMnO_4$ to AP increases, the samples progressively darken. At the ratios of 60:40 and 80:20, the $KMnO_4$ particles become visible on the surface of the sample, as shown in Fig. 6 (c) and 6 (d), respectively. The dark color is a result of the inclusion of $KMnO_4$/AP as a dual oxidiser, and their composition is the primary factor contributing to the color. In addition, it was observed that the black color appeared evenly, indicating that the $KMnO_4$/AP

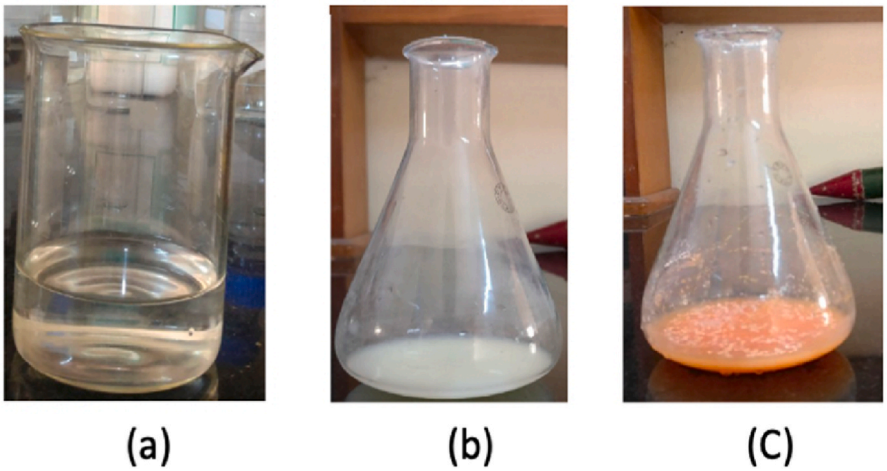

Fig. 5. Colour references of (a) Water sample (b) Midpoint titration and (c) End-point titration (Vellaisamy and Biswas, 2020). (For interpretation of the references to color in this figure legend, the reader is referred to the Web version of this article.)

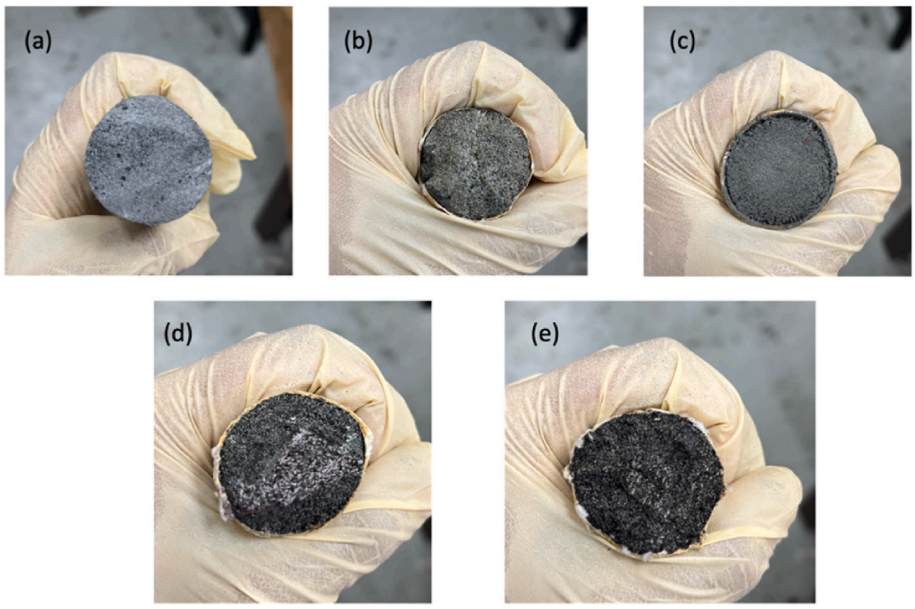

Fig. 6. Physical condition of (a) AP, (b) $KMnO_4$/AP (20:80), $KMnO_4$/AP (40:60), $KMnO_4$/AP (60:40), $KMnO_4$/AP (80:20) based composite solid propellant.

mixture was uniformly distributed in the CSP systems for all the samples.

3.1.2. Morphological and elemental composition analysis of composite solid propellant (CSP) with dual oxidiser ($KMnO_4$/AP) based

This experimental study focuses on capturing images of propellant samples at a magnification of 200X to analyse their morphological structure. As illustrated in Fig. 7, all the samples displayed typical characteristics of AP-based CSP, indicating the success combination of binder and oxidiser. The observed morphological structures align closely with the experimental data reported by Kosiba et al. (2017). In Fig. 7 (a), the white spherical particles visible on the surface correspond to the oxidiser particles, which are enclosed by a polymer binder called hydroxy-terminated polybutadiene (HTPB). This polymer binder exhibits a rubbery matrix structure that effectively retains and interacts with AP particles. The analysis of this interface enabled the assessment of binder-AP adhesion, interfacial interactions, and the identification of any interfacial layers or phases (Kosiba et al., 2017). Furthermore, establishing a robust and consistent binder-AP interface is crucial for ensuring effective energy transfer during combustion. Additionally, Fig. 7 (b) illustrates the presence of a rubbery structure on the surface of the propellant, particularly at the interface between $KMnO_4$ and AP. The HTPB imparts a significant level of flexibility, while the binder primarily serves to hold the solid $KMnO_4$/AP particles together, resulting in a brittle structural condition. The formation of cracks at the interface between $KMnO_4$ and AP, indicated by the blue circle, clearly demonstrates this phenomenon, arising from the inclusion of 20 % $KMnO_4$ interspersed between the AP particles and the HTPB matrix in this rod-like solid structure. Kosiba et al. (2017) claimed that crack formation in HTPB has been attributed to matrix tearing and interfacial debonding between the binder matrix and solid particles. These findings suggest that factors like matrix brittleness and interfacial weaknesses contribute significantly to crack development in HTPB-based CSP.

As the concentration of $KMnO_4$ increases, its rod-like structure becomes more visible, as seen in Fig. 7 (c). Notably, the $KMnO_4$/AP sample with a 40:60 ratio demonstrates a noticeably smoother surface compared to the 20:80 ratio sample. The smoother areas may indicate regions where the binder encapsulates the oxidiser particles, whereas the rough or jagged sections likely represent the exposed surfaces of crystalline $KMnO_4$ and AP.

Furthermore, the size of AP particles decreases from approximately 100 μm–50 μm, while the $KMnO_4$ structure also becomes more compact. This size reduction, mainly caused by crashing and grinding in $KMnO_4$ AP mixing process using agate mortar. This reduction in AP particle size also makes observation more challenging, as the particles were smaller and exhibited a flatter morphology compared to their original spherical shape. The $KMnO_4$/AP (60:40) sample exhibits a morphological structure analogous to that of the $KMnO_4$/AP (40:60) sample, resulting in an even more compact configuration, as illustrated in Fig. 7 (d). This increased compactness enhances burning efficiency, given that the pores in the CSP surface structure significantly influence combustion performance. By increasing the $KMnO_4$ to AP ratio, the visibility of the $KMnO_4$ structure is enhanced, while the AP particles appear to diminish. In this sample, the predominance of $KMnO_4$ contributes to improved ductility of the HTPB matrix by retaining a greater quantity of $KMnO_4$/AP. However, this may also lead to the formation of voids, as illustrated in Fig. 7 (e), at the interface between the solid particles and the HTPB matrix. Kosiba et al. (2017) noted that these interfacial gaps or voids could negatively impact the material's thermal characteristics and combustion rate performance.

Fig. 7 also presents the EDX mapping results along with the elemental composition intensity graph for the entire microstructural surface of each sample. The samples for these tests were taken from the surface of the composite structure. The primary elements identified in the AP-based CSP were carbon (C), hydrogen (H), oxygen (O), nitrogen (N), aluminium (Al), and chlorine (Cl). As previously discussed, the O, N, H, and Cl were derived from the AP, while C and Al originated from the HTPB and aluminium powder, respectively.

It can be observed that as the weight percentage of $KMnO_4$ to AP increases, the detected oxygen weight percentage remains constant across all samples. The oxygen content varies between 19.5 % and 20 %, indicating no significant changes with the rising $KMnO_4$ to AP ratio. Besides, the incorporation of $KMnO_4$ into the AP-based CSP system introduces potassium (K) and manganese (Mn), elements that come from $KMnO_4$. The presence of these elements proves that $KMnO_4$ is well mixed into the AP-based CSP system, as previously discussed in the SEM analysis. Both K and Mn showed an increase in weight percentage as the $KMnO_4$ to AP ratio rises, which is visually evident from the darkening purple color of the CSP sample. Furthermore, a decrease in the weight percentage of chlorine (Cl) is observed with the increased $KMnO_4$ to AP ratio. In the AP-based CSP system, the initial Cl composition is 11.12 %. As $KMnO_4$ is added at a ratio of 20:80, 40:60, 60:40, and 80:20, the Cl element diminished to 8.22 %, 5.29 %, 3.59 %, and 1.98 %, respectively.

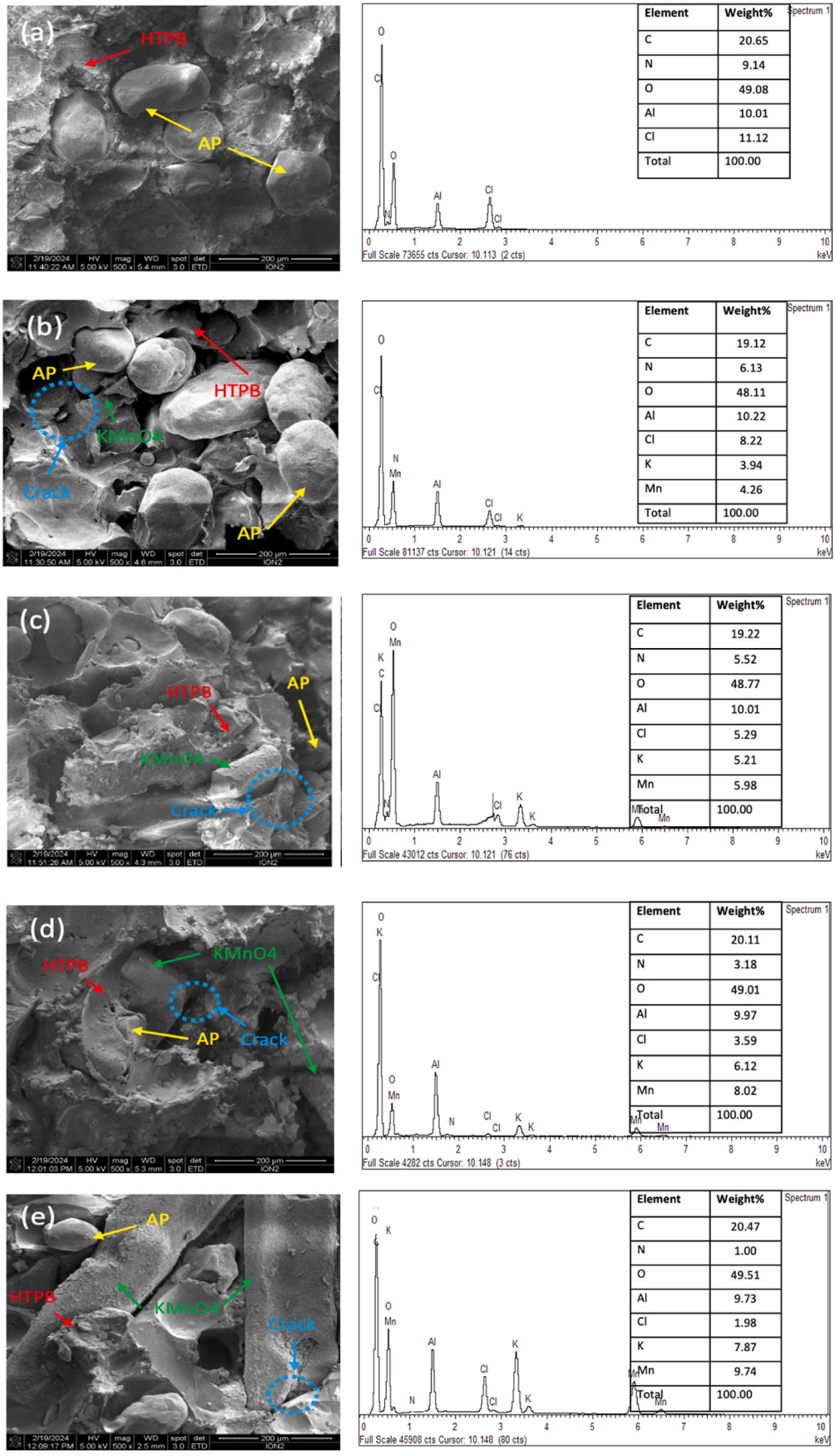

Fig. 7. Morphological structure image and elemental composition plot of (a) AP, (b) $KMnO_4$/AP (20:80), (c) $KMnO_4$/AP (40:60), (d) $KMnO_4$/AP (60:40), (e) $KMnO_4$/AP (80:20) composite solid propellant based.

This interesting finding can be attributed to the minimum amount of AP usage, as Cl is solely sourced from it. Trache et al. (2017b) stated that theoretically, when the less element of Cl is used in the propellant composition, the less HCl gases will be produced as combustion by-products. This finding aligns with the research objective of minimising HCl, a toxic gas from the combustion product of AP-based CSP systems. Furthermore, as mentioned in the previous subchapter, while the low atomic number of hydrogen (H) prevents its detection in EDX analysis, it still exists and is contributed by the binder and curing agent.

3.2. Catalytic properties study of $KMnO_4$/AP

3.2.1. Thermal decomposition analysis of composite solid propellant (CSP) with dual oxidiser ($KMnO_4$/AP) based

In Fig. 8 (a), the TGA curve reveals three stages of thermal decomposition occurring at temperatures ranging from 100 to 1000 °C. Each stage corresponds to different reactions within the propellant sample, leading to noticeable endothermic and exothermic peaks on the DSC curve, as discussed by Fertassi et al. (2023). The transition of AP from an orthorhombic to a cubic crystalline phase is marked by an endothermic peak at 235.27 °C. Additionally, the breakdown of residual HTPB contributes to an exothermic peak within the temperature range of 440–500 °C, and a modest exothermic peak in this temperature range results from the oxidation of Al particles (Sun et al., 2022).

Based on Fig. 8 (b), the weight loss percentages of all samples behaved similarly to the AP-based CSP sample, with the exceptions of $KMnO_4$/AP CSP (20:80) and $KMnO_4$/AP CSP (40:60). Both $KMnO_4$/AP CSP (20:80) and $KMnO_4$/AP CSP (40:60) exhibit only one significant weight loss peak at the onset temperature. In contrast, the other samples follow the typical TGA behaviour of AP CSP, characterised by two distinct weight loss points. This difference in the number of weight loss points represents that the $KMnO_4$/AP CSP (20:80) and $KMnO_4$/AP CSP (40:60) samples have only one exothermic peak during the overall thermal decomposition process, unlike the other samples.

This phenomenon is further illustrated in the DSC plot in Fig. 8 (c), where it can be clearly seen that the onset temperatures for both $KMnO_4$/AP CSP (20:80) and $KMnO_4$/AP CSP (40:60) occurred at earlier temperatures than the main weight loss points but later than the onset temperatures of the other samples, specifically at 331.32 °C and 352.34 °C, respectively. The $KMnO_4$/AP CSP (40:60) sample exhibits a lower onset temperature compared to $KMnO_4$/AP CSP (20:80), indicating that its thermal decomposition occurs at a lower temperature.

As the weight loss continues, the onset temperature gradually decreases until the sample reaches 0 % weight loss, signifying the completion of the decomposition process for all compositions. Meanwhile, $KMnO_4$/AP CSP (60:40) and $KMnO_4$/AP CSP (80:20) samples demonstrate two distinct weight loss points, similar to the AP CSP sample, with $KMnO_4$/AP CSP (60:40) occurring at a lower temperature than both AP CSP and $KMnO_4$/AP CSP (80:20) samples. The observed shift of weight loss temperatures to a lower temperature indicates that, with increasing amounts of $KMnO_4$ in the AP CSP system with $KMnO_4$ to AP ratios of 20:80, 40:60, 60:80, the thermal decomposition occurs at lower temperatures. However, as the ratio of $KMnO_4$ increases to 80 %, the results show an opposite effect, as this sample exhibits higher weight loss temperatures at all points, indicating enhanced thermal stability. However, the $KMnO_4$/AP (80:20) sample is thermally more stable, meaning it can withstand higher temperatures without breaking down prematurely compared to others. Yuan et al. (2021) assert that the reduction in weight loss temperature for catalysed AP CSP is due to the catalyst's ability to decrease the activation energy, thereby enhancing reaction kinetics and accelerating the thermal decomposition rate, which ultimately improves the propellant's overall efficiency. This research demonstrates that $KMnO_4$ functions as a catalyst in the combustion process of the AP CSP system by reducing the thermal decomposition temperature. The experimental findings concerning the reduction of the onset decomposition temperature align with those of

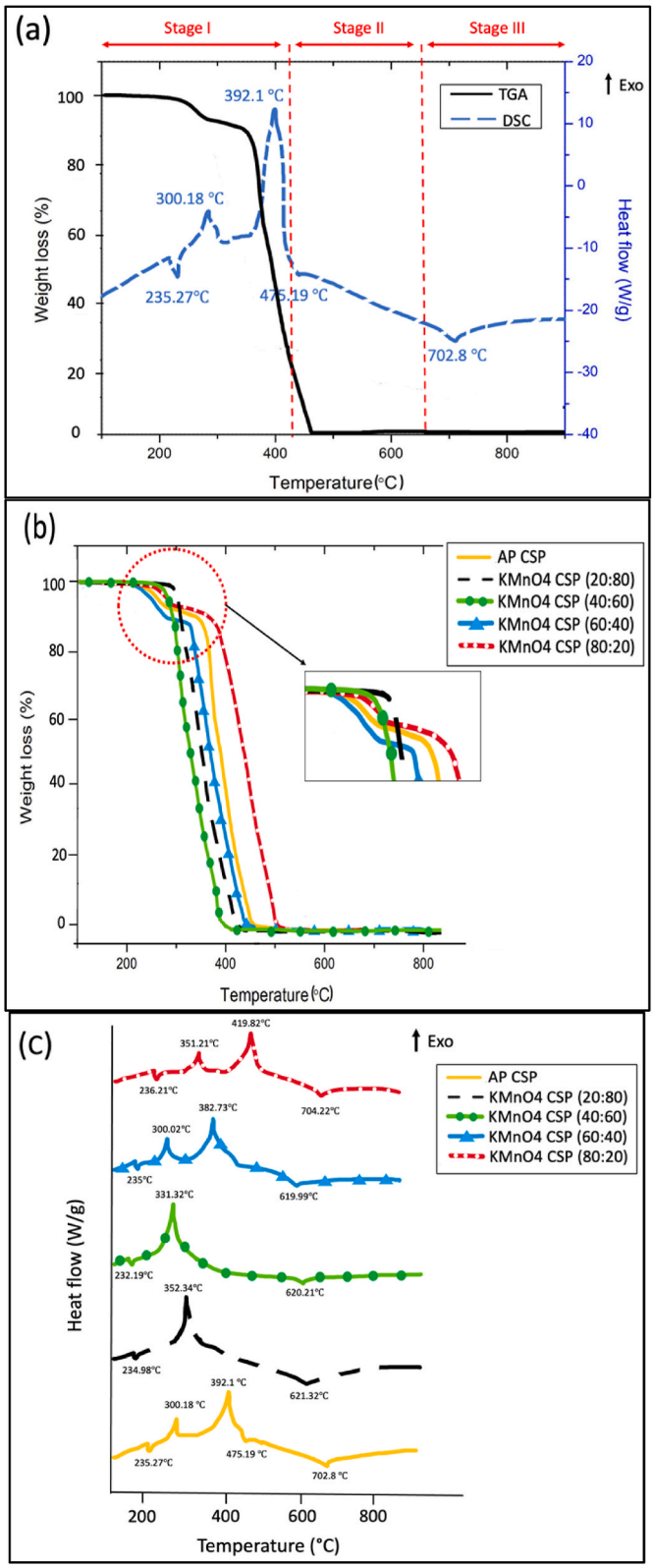

Fig. 8. (a) TGA and DSC result of samples AP based CSP, (b) TGA plotting results of samples AP and $KMnO_4$/AP based CSP, and (c) DSC plotting results of samples AP and $KMnO_4$/AP with different ratios based CSP.

Yang et al. (2024), who demonstrated that incorporating the highly catalytic active α-Fe_2O_3 into an AP/HTPB-based CSP system decreases the onset decomposition temperature, resulting in a singular weight loss point.

Fig. 8 (c) illustrates the DSC plot for all samples, revealing that the $KMnO_4$/AP CSP samples with ratios of 60:40 and 80:20 exhibit behaviour similar to that of AP CSP. In contrast, the $KMnO_4$/AP CSP with ratios of 20:80 and 40:60 resulted in a different trend, aligning with the results from the TGA curve discussed earlier. Specifically, the $KMnO_4$/AP CSP samples at the 60:40 and 80:20 ratios show the same behaviour as AP CSP, characterised by an initial endothermic peak followed by two exothermic peaks, concluding with an endothermic peak corresponding to aluminium melting phase.

Meanwhile, the $KMnO_4$/AP CSP samples at ratios of 20:80 and 40:60 resulted in one initial endothermic peak and a main exothermic peak, ended with one aluminium endothermic peak melting phase. There are no significant changes observed in the first endothermic peak across all samples. However, the second exothermic peak shows notable differences, while the first exothermic peak varies only slightly. Notably, in the temperature range of 300 °C–410 °C, two exothermic peaks which indicate presence of the low temperature decomposition (LTD) and high temperature decomposition (HTD) was found to merge into a single exothermic peak for the $KMnO_4$/AP CSP samples at ratios of 20:80 and 40:60. This merging suggests that the catalytic effect of $KMnO_4$ may lead to overlapping or simultaneous reactions associated with LTD and HTD. As previously mentioned, $KMnO_4$ acts as a catalyst for the decomposition of AP, potentially lowering the activation energy for both decomposition steps and causing them to occur simultaneously at one time. Yang et al. (2024) reported that when one reaction releases heat, it can trigger or speed up the other, effectively merging the two thermal events into one. This interesting result is similar to the experimental data by Wang et al. (2019), where the DSC results of AP catalysed with Cu metal–organic framework (Cu-MOF) and carbon nanomaterials also demonstrated the merging of two exothermic peaks. The data of the DSC curves have been tabulated in Table 3 to illustrate the changes in LTD and HTD of all the $KMnO_4$/AP CSP samples compared to AP CSP as well as their heat release.

In addition, the merged exothermic peak observed in the $KMnO_4$/AP CSP samples with ratios of 20:80 and 40:60 shifted the HTD of AP CSP from 392.10 °C to 352.34 °C and 331.32 °C, respectively. Among these, the $KMnO_4$/AP CSP (40:60) sample exhibited the most significant catalytic effect on AP decomposition, lowering the HTD value to a greater extent than the $KMnO_4$/AP CSP (20:80) sample. This is followed by the $KMnO_4$/AP CSP (60:40) and $KMnO_4$/AP CSP (80:20) samples, with the latter showing a lesser reduction in HTD, which is critical as HTD represents the primary stage of the AP CSP decomposition process.

As noted in Table 3, the $KMnO_4$/AP CSP (20:80) and $KMnO_4$/AP CSP (40:60) samples do not exhibit LTD due to the merging of their two exothermic peaks. Furthermore, the $KMnO_4$/AP CSP (60:40) sample reduced both LTD and HTD of AP CSP to 300.02 °C and 382.73 °C, respectively. In contrast, the $KMnO_4$/AP (80:20) sample increased both LTD and HTD, raising them from 300.18 °C to 392.10 °C–351.21 °C and 419.82 °C, as illustrated in Table 3.

The decrease in HTD indicates that $KMnO_4$ acts as a catalyst, providing an alternative reaction pathway with a lower activation energy barrier. Park et al. (2020) mentioned that by lowering this barrier, the catalyst facilitates the AP decomposition reaction, allowing it to proceed at lower temperatures. This is evidenced by the heat release value of the $KMnO_4$/AP CSP (40:60) sample, which increased from 1929.1 J/g to 3721.2 J/g. This rise in heat release value enhances the overall system's tendency to decompose at lower temperatures (Cegla et al., 2019). Moreover, the merging of the two exothermic peaks, as previously discussed, results in a significant release of heat. This released heat can locally elevate the temperature of the reaction, further accelerating the decomposition process. Thus, it is suggested that the $KMnO_4$/AP CSP (40:60) sample demonstrated the best catalytic performance as a dual oxidiser in AP-based CSP system.

3.2.2. *Energetic properties (density and heat of combustion) of composite solid propellant (CSP) with dual oxidiser ($KMnO_4$/AP) based*

An effective propellant formulation optimises the heat release to produce the highest possible specific impulse (I_{sp}), which serves as is a measure of the rocket motor's efficiency. A higher heat release enhances the combustion temperature, thereby increasing the exhaust gas velocity through the nozzle, which directly results in a higher specific impulse (I_{sp}) and improved propulsion efficiency of the solid rocket motor (Yuan et al., 2021). Table 4 summarises the results of the $KMnO_4$ effect on the heat of combustion in AP-based CSP.

The results presented in Table 4 indicate that all samples exhibit a constant heat of combustion value ranging from 1247.0 cal/g to 1254.01 cal/g. The heat of combustion for the CSP samples exhibits a slight increase with the incorporation of KMnO4 into AP, reaching its peak at a 40:60 ratio. However, at the ratios of 60:40 and 80:20, the heat of combustion values decreases to 1249.65 cal/g and 1247.73 cal/g, respectively. Besides, the highest heat of combustion was observed in the KMnO4/AP sample with a ratio of 40:60, which corresponds to the highest combustion efficiency percentage at 100.2 % compared to the other samples. The observed combustion efficiency exceeding 100 % is due to minor experimental errors, which are calorimeter calibration inaccuracies and sensor precision limitations, which may have led to a slight overestimation of energy output. Additionally, potential secondary reactions involving $KMnO_4$ could have contributed to unexpected heat release, highlighting the need for further investigation and refinements in measurement accuracy. Besides, Yang et al. (2024) also had experienced the same situation where they tested the calorific value of highly catalytic active α-Fe_2O_3-Carbon Nanotube CSP. This indicates that the KMnO4/AP (40:60) sample releases more energy, resulting in higher temperatures and pressures within the combustion chamber, ultimately leading to higher exhaust velocities. This relationship arises because the exhaust velocity is directly related to the energy released during the combustion process (Boulkadid et al., 2020). Moreover, a higher heat of combustion means that more energy is available per unit mass of fuel.

Table 3
Low temperature decomposition (LTD), high temperature decomposition (HTD) and heat release (△H) result of AP and $KMnO_4$/AP based CSP with different ratios.

Sample	LTD/°C	HTD/°C	△H (J/g)
AP CSP	300.18	392.1	1929.1
$KMnO_4$/AP (20:80) CSP	–	352.34	2319.8
$KMnO_4$/AP (40:60) CSP	–	331.32	3721.2
$KMnO_4$/AP (60:40) CSP	300.02	382.73	1876.0
$KMnO_4$/AP (80:20) CSP	351.21	419.82	1862.3

Table 4
Effects of $KMnO_4$ with different ratios on the energetic properties of AP based CSP.

CSP Samples	Mass of the samples(g)	Heat of combustion (cal/g)	Combustion efficiency (%)
AP CSP	28	1247	99.70
$KMnO_4$/AP (20:80) CSP	28	1250.98	99.9
$KMnO_4$/AP (40:60) CSP	28	1254.01	100.2
$KMnO_4$/AP (60:40) CSP	28	1249.65	99.8
$KMnO_4$/AP (80:20) CSP	28	1247.73	99.6

3.3. HCl concentration analysis in the combustion product of composite solid propellant (CSP) with dual oxidiser ($KMnO_4$/AP) based

The concentration of chloride in the concentration of water samples was determined using Mohr's titration technique, which employed a standard solution of silver nitrate ($AgNO_3$) to precipitate chloride ions as silver chloride (AgCl). During this titration, hydrochloric acid (HCl) reacts with silver nitrate, where the chloride ions from HCl interact with silver ions (Ag^+) from the silver nitrate, resulting in the formation silver chloride (AgCl) precipitate. The stoichiometric reaction between silver nitrate and hydrochloric acid can be described as follows:

$$AgNO_3\ (aq) + HCl\ (aq) = AgCl\ (s) + HNO_3\ (aq) \quad (6)$$

The stoichiometric ratio is 1:1, indicating that 1 mol of HCl reacts with 1 mol of $AgNO_3$ to produce 1 mol of AgCl and 1 mol of HNO_3. The $AgNO_3$ solution was added constantly from a pipette until the first permanent reddish-brown colour appeared. This colour change indicates the formation of silver chromate (Ag_2CrO_4) and marks the endpoint of the titration. The endpoint is detected by the formation of a reddish-brown precipitate of silver chromate (Ag_2CrO_4) as follows:

$$2Ag\ (aq) + {CrO_4}^{2-}\ (aq) \rightarrow Ag_2CrO_4\ (s) \quad (7)$$

Once the chloride ions have reacted with the silver ions to form silver chloride (AgCl), the reaction reaches completion. Fig. 9 shows the process, displaying the initial-point water sample with K_2CrO_4 as indicator, mid-point, and endpoint of the titration.

When $KMnO_4$ reacts with AP, it undergoes a highly exothermic oxidation-reduction which is a redox reaction. This reaction produces various compounds formed from the decomposition and recombination of elements present in the reactants. It serves as a classic example of a redox process, with $KMnO_4$ acting as the oxidising agent and NH_4ClO_4 provides both fuel and additional oxidiser components. The stoichiometry equation for the reaction between $KMnO_4$ and AP during the combustion process is as follows:

$$2KMnO_4 + 2NH_4ClO_4 \rightarrow 2KCl + 2MnO_2 + 4H_2O + 4O_2 + N_2 \quad (8)$$

The newly developed dual oxidiser $KMnO_4$/AP altered only the physical structure of both compositions without affecting the chemical elements. Consequently, from the stoichiometry reaction, the combustion of the dual oxidiser $KMnO_4$/AP with 2 mol of $KMnO_4$ and 2 mol of AP produced 2 mol of potassium chloride (KCl), 2 mol of manganese dioxide (MnO_2), 4 mol of water (H_2O), 4 mol of oxygen gas (O_2), and 1 mol of nitrogen gas (N_2). KCl has a high melting point of about 770 °C (1420 °F). The potassium (K) in $KMnO_4$ scavenges the HCl to form KCl. Usually, in AP-based CSP systems, combustion temperatures mainly reach about 1500 °C–2500 °C, potentially reaching or exceeding the melting point of KCl. Thus, it will be in the form of gas. The Cl elements in the combustion of $KMnO_4$/AP originate from KCl, which this element is not considered a highly toxic gas (Wang et al., 2019) compared to HCl gases, which the conventional AP-based CSP produces. The chloride content data obtained from Mohr's titration method were tabulated in Table 5.

Table 5
Result of chlorine content from the Mohr's titration method.

CSP Samples	Volume level of silver nitrate ($AgNO_3$) solution used (ml)	Average volume level of silver nitrate ($AgNO_3$) solution used (ml)	Chloride content (ppm)
AP CSP	2.16 2.01 2.13	2.1	745.5
$KMnO_4$/AP (20:80) CSP	1.95 1.94 1.90	1.93	685.15
$KMnO_4$/AP (40:60) CSP	1.31 1.28 1.25	1.28	454.41
$KMnO_4$/AP (60:40) CSP	1.12 1.10 1.08	1.10	390.54
$KMnO_4$/AP (80:20) CSP	0.92	0.87	311.22

Based on Table 5, all samples exhibited chlorine content values ranging from 311.22 to 745.5 ppm. The conventional AP-based CSP showed the highest chlorine content at 745.5 ppm compared to the other samples. However, with the incorporation of $KMnO_4$ into the AP-based CSP system, a notable reduction in chlorine content was observed as the ratio of $KMnO_4$ to AP increased. At a ratio of 60:40, the chlorine content decreased significantly to 390.54 ppm, nearly half the value observed in the conventional AP-based CSP. Furthermore, the $KMnO_4$/AP sample with $KMnO_4$ to AP ratio of 80:20 resulted in the highest reduction in chlorine content with a value of 311.22 ppm. Table 6 illustrates the percentage reductions in chlorine content value for the $KMnO_4$/AP CSP samples with different ratios from the conventional AP-based CSP.

Referring to Tables 6 and it is evident that the chlorine content increases with a higher ratio of $KMnO_4$ to AP. The $KMnO_4$/AP sample with a 60:40 ratio demonstrates a substantial reduction of nearly 50 %, while the sample with an 80:20 ratio resulted in the highest chlorine content reduction at 58.25 %. This elucidates that increasing the amount of $KMnO_4$ in the propellant composition effectively reduces chlorine content in combustion by-products by reducing the use of AP, which is the primary contributor to HCl gas production. Additionally, the bar chart in Fig. 10 visualises the comparison of chlorine content results from

Table 6
Percentage reduction from the pure AP CSP.

Composite solid propellant sample	Chlorine content reduction (%)
AP CSP	–
$KMnO_4$/AP (20:80) CSP	8.10
$KMnO_4$/AP (40:60) CSP	39.04
$KMnO_4$/AP (60:40) CSP	47.62
$KMnO_4$/AP (80:20) CSP	58.25

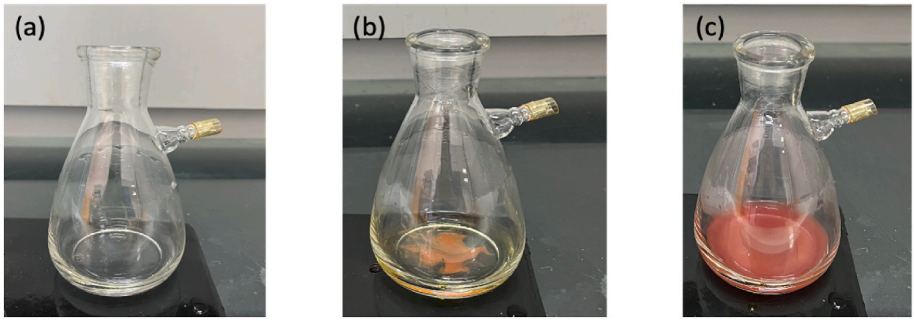

Fig. 9. The result of the water sample at (a) initial-point, (b) Mid-point, (c) endpoint of Mohr's titration.

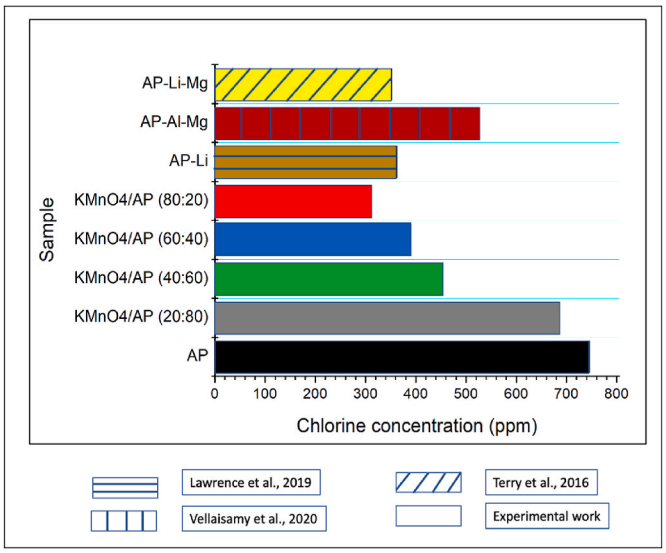

Fig. 10. Bar chart comparison result of CSP samples chlorine concentration value in this experimental work with literature.

literature study with those from this research work.

The bar chart in Fig. 10 illustrates that several CSP samples made by Lawrence et al. (2019), Vellaisamy et al. (Vellaisamy and Biswas, 2020), and Terry et al. (2016) revealed noteworthy results in reducing chlorine content as a combustion by-product. The $KMnO_4$/AP sample with a 60:40 ratio shows a chlorine concentration mostly similar to the AP-Li-Mg sample developed by Terry et al. (Yildiz et al.). Interestingly, the $KMnO_4$/AP sample with ratio of 80:20 exhibits a lower chlorine concentration than all other samples and nearly doubles the reduction achieved with conventional AP-based CSP. While lithium-based propellant samples generally demonstrate superior performance, they cannot be classified as green propellants due to the discharge of poisonous lithium chloride in their exhaust. Additionally, the handling of highly reactive lithium-based propellant poses significant challenges. In contrast, the novel $KMnO_4$/AP composition with ratio of 80:20, is promising as a dual oxidiser CSP formulation, as it minimises chlorine content as a combustion by-product and produces KCl.

4. Conclusions and future recommendation studies

The investigation on how the inclusion of $KMnO_4$ affects AP-based CSP in terms of material characterisation, catalytic properties, and HCl reduction as combustion by-product has been elucidated with different $KMnO_4$ to AP ratios. The following conclusions are drawn based on the data obtained from experimental works:

i) When $KMnO_4$ was introduced, the CSP exhibited a darker appearance, and the surface of the samples became rougher as the ratio of $KMnO_4$ to AP increased. Besides, morphological analysis reveals that an increase in the ratio of $KMnO_4$ to AP results in a more distinct observation of the rod-like structure of $KMnO_4$. The size of AP particles decreases from around 100 μm–50 μm, while the structure of $KMnO_4$ similarly grows shorter.

ii) The CSP system shows that the $KMnO_4$/AP (40:60) sample performs the best in terms of catalytic properties, since it lowers the HTD value of AP from 392.1 °C to 331.32 °C. Moreover, this sample also exhibits the greatest heat of combustion value of 1254.01 cal/g.

iii) A higher ratio of $KMnO_4$/AP results in a higher percentage of decrease in chlorine concentration. The $KMnO_4$/AP sample with a ratio of 60:40 exhibited a significant decrease of nearly 50 %, while the sample with a ratio of 80:20 resulted in the largest reduction in chlorine content, with a value of 58.25 %.

For future studies, it is recommended to examine the burn rate performance and thrust evaluation test of the novel KMnO4/AP dual oxidiser. It is a critical parameter in rocket propellant to ensure the newly developed oxidiser does not compromise the performance in terms of burn rate properties, thrust value, and specific impulse. Besides, the mechanical properties of the KMnO4/AP CSP also need to be evaluated to ensure the propellant can sustain in various operation pressure regimes and meet the standard.

CRediT authorship contribution statement

Izzat Najmi Yaacob: Writing – original draft, Visualization, Software, Resources, Project administration, Methodology, Investigation, Conceptualization. **Ezanee Gires:** Validation, Supervision, Investigation. **Adi Azrif Basri:** Supervision, Formal analysis, Data curation, Conceptualization. **Kamarul Arifin Ahmad:** Visualization, Validation, Software, Resources, Project administration, Funding acquisition, Formal analysis. **Kamsani Kamal:** Resources, Methodology, Investigation. **Nor Afizah Salleh:** Supervision, Methodology, Formal analysis. **Suraya Shahedi:** Visualization, Validation, Formal analysis, Data curation. **Fikri Rasih:** Resources, Formal analysis, Data curation. **Zakwan Azizi:** Visualization, Validation, Methodology. **Sharul Sham Dol:** Supervision, Funding acquisition, Conceptualization. **Norkhairunnisa Mazlan:** Writing – review & editing, Validation, Supervision, Resources, Project administration, Investigation, Formal analysis, Conceptualization.

Funding

This work was supported by Ministry of Science, Technology, and Innovation (MOSTI), Malaysia, [FRGS/1/2024/TK09/UPM/02/1].

Declaration of competing interest

The authors declare the following financial interests/personal relationships which may be considered as potential competing interests: Norkhairunnisa Mazlan reports financial support was provided by Ministry of Science Technology and Innovation. If there are other authors, they declare that they have no known competing financial interests or personal relationships that could have appeared to influence the work reported in this paper.

Acknowledgements

The authors thank the staff of Science & Technology Research Institute for Defence (STRIDE) for providing support in completing the experimental works, in particular the director of the rocket and propulsion department ChM. Nor Afizah Salleh.

Data availability

The data has been included in the PDF of the research manuscript submitted

References

Abdelhafiz, M., Yehia, M., Mostafa, H.E., Wafy, T., 2021. Self-catalyzed nanoscale ammonium perchlorate for advanced composite solid rocket propellant. Nano Express 2 (3), 030008. https://doi.org/10.1088/2632-959X/ac2568.

Adeniyi, G.O., Nkere, I., Adetoro, L.M., Sholiyi, O.S., 2021. Performance analysis of a dual-fuel sugar-based solid rocket propellant. Eur. J. Eng. Technol. Res. 6 (2), 34–41. https://doi.org/10.24018/ejeng.2021.6.2.2347.

Bogusz, R., Magnuszewska, P., 2019. The aging studies of the low HCl content composite rocket propellant. Propellants, Explos. Pyrotech. 44 (9), 1193–1198. https://doi.org/10.1002/prep.201900074.

Boulkadid, K.M., Trache, D., Krai, S., Lefebvre, M.H., Jeunieau, L., Dejeaifve, A., 2020. Estimation of the ballistic parameters of double base gun propellants. Propellants, Explos. Pyrotech. 45 (5), 751–758. https://doi.org/10.1002/prep.201900341.

Cegla, M., Zmywaczyk, J., Koniorczyk, P., 2019. Thermo-mechanical analysis of heterogeneous solid rocket propellant. Issues Armament Technol 147 (3), 105–121. https://doi.org/10.5604/01.3001.0012.8315.

Chalghoum, F., Trache, D., Maggi, F., Benziane, M., 2020. Effect of complex metal hydrides on the elimination of hydrochloric acid exhaust products from high-performance composite solid propellants: a theoretical analysis. Propellants, Explos. Pyrotech. 45 (8), 1204–1215. https://doi.org/10.1002/prep.201900408.

Chen, Y., Ma, K., Wang, J., Gao, Y., Zhu, X., Zhang, W., 2018. Catalytic activities of two different morphological nano-MnO_2 on the thermal decomposition of ammonium perchlorate. Mater. Res. Bull. 101, 56–60. https://doi.org/10.1016/j.materresbull.2018.01.013.

D'Andrea, B., Lillo, F., Faure, A., Perut, C., 2000. A new generation of solid propellants for space launchers. Acta Astronaut. 47 (2–9), 103–112. https://doi.org/10.1016/S0094-5765(00)00049-7.

de Flon, J., Andreasson, S., Liljedahl, M., Oscarson, C., Wanhatalo, M., Wingborg, N., 2011. Solid propellants based on ADN and HTPB. In: 47th AIAA/ASME/SAE/ASEE Joint Propulsion Conference & Exhibit, 6136. https://doi.org/10.2514/6.2011-6136.

DeLuca, L.T., Shimada, T., Sinditskii, V.P., Calabro, M., Manzara, A.P., 2017. An introduction to energetic materials for propulsion. In: Chemical Rocket Propulsion: A Comprehensive Survey of Energetic Materials, pp. 3–59. https://doi.org/10.1007/978-3-319-27748-6_1.

DeLuca, L.T., Bohn, M.A., Gettwert, V., Weiser, V., Tagliabue, C., 2018. Innovative solid rocket propellant formulations for space propulsion. In: Energetic Materials Research, Applications, and New Technologies. IGI Global, pp. 1–24. https://doi.org/10.4018/978-1-5225-2903-3.ch001.

Doll, D.W., Lund, G.K., 1992a. Magnesium-neutralized propellant. J. Propul. Power 8 (6), 1185–1191. https://doi.org/10.2514/3.11460.

Doll, D.W., Lund, G.K., 1992b. Magnesium-neutralized propellant. J. Propul. Power 8 (6), 1185–1191. https://doi.org/10.2514/3.11460.

Fahd, A., Dubois, C., Chaouki, J., Wen, J.Z., Youssef, E., 2021. Synthesis and characterization of tertiary nanothermite CNMs/Al/KClO4 with enhanced combustion characteristics. Propellants, Explos. Pyrotech. 46 (6), 995–1005. https://doi.org/10.1002/prep.202000222.

Fertassi, M.A., Belkhiri, S., Touidjine, S., Hamdane, A., Kechit, H., Boulkadid, M.K., Khimeche, K., 2023. Enhancing the thermal decomposition of composite modified double base propellant using Al/hematite and Al/Hematite/Graphene thermites. React. Kinet. Mech. Catal. 136 (6), 3127–3149. https://doi.org/10.1007/s11144-023-02507-8.

Gańczyk-Specjalska, K., Paziewska, P., Bogusz, R., Lewczuk, R., Cieślak, K., Uszyński, M., 2021. Performance and sensitivity properties of solid heterogeneous rocket propellant based on a binary system of oxidisers (PSAN and AP). Processes 9 (12), 2201. https://doi.org/10.3390/pr9122201.

Garino, S., Antonaci, P., Pastrone, D., Sangermano, M., Maggi, F., 2021. Photo-polymerization for additive manufacturing of composite solid propellants. Acta Astronaut. 182, 58–65. https://doi.org/10.1016/j.actaastro.2021.01.062.

Hamim, N., Aristiawan, Y., Hindayani, A., Andreas, A., Komalasari, I., 2023. Method verification for determination of sodium chloride purity: a comparison of potentiometric and Mohr titration. In: AIP Conf. Proc., 2902. https://doi.org/10.1063/5.0173420, 1.

He, Z., Xia, Z., Hu, J., Li, Y., 2019. Lithium-perchlorate/polyvinyl-alcohol-based aluminized solid propellants with adjustable burning rate. J. Propul. Power 35 (3), 512–519.

Klapötke, T.M., Minar, N.K., Stierstorfer, J., 2009. Investigations of bis (methyltetrazolyl) triazenes as nitrogen-rich ingredients in solid rocket propellants—synthesis, characterization, and properties. Polyhedron 28 (1), 13–26. https://doi.org/10.1016/j.poly.2008.09.015.

Kopacz, W., Okninski, A., Kasztankiewicz, A., Nowakowski, P., Rarata, G., Maksimowski, P., 2022. Hydrogen peroxide—a promising oxidiser for rocket propulsion and its application in solid rocket propellants. FirePhysChem 2 (1), 56–66. https://doi.org/10.1016/j.fpc.2022.03.009.

Kosiba, G.D., Wixom, R.R., Oehlschlaeger, M.A., 2017. High-fidelity microstructural characterization and performance modeling of aluminized composite propellant. Propellants, Explos. Pyrotech. 42 (12), 1387–1395. https://doi.org/10.1002/prep.201700124.

Lawrence, A.R., Laktas, J.M., Place, G.J., Jelliss, P.A., Buckner, S.W., Sippel, T.R., 2019. Organically-capped, nanoscale alkali metal hydride and aluminium particles as solid propellant additives. J. Propul. Power 35 (4), 736–746. https://doi.org/10.2514/1.B37409.

Maggi, F., Carlotti, S., Nichelini, L., Masini, A., Adorno, M., Galavotti, A., Neri, A., 2023a. Quantification of HCl in solid propellant combustion products. In: AIAA Scitech 2023 Forum, 1515. https://doi.org/10.2514/6.2023-1515.

Maggi, F., Carlotti, S., Nichelini, L., Masini, A., Adorno, M., Galavotti, A., Neri, A., 2023b. Quantification of HCl in solid propellant combustion products. In: AIAA Scitech 2023 Forum, 1515. https://doi.org/10.2514/6.2023-1515.

Najser, T., Gaze, B., Knutel, B., Verner, A., Najser, J., Mikeska, M., Němček, O., 2022. Analysis of the effect of catalytic additives in the agricultural waste combustion process. Mater 15 (10), 3526. https://doi.org/10.3390/ma15103526.

Okniński, A., Nowakowski, P., Kasztankiewicz, A., 2020. Survey of low-burn-rate solid rocket propellants. In: Innovative Energetic Materials: Properties, Combustion Performance and Application, pp. 313–349. https://doi.org/10.1007/978-981-15-4831-4_11.

Pang, W., Li, Y., DeLuca, L.T., Liang, D., Qin, Z., Liu, X., Fan, X., 2021. Effect of metal nanopowders on the performance of solid rocket propellants: a review. Nanomaterials 11 (10), 2749. https://doi.org/10.3390/nano11102749.

Park, S., Choi, S., Kim, K., Kim, W., Park, J., 2020. Effects of ammonium perchlorate particle size, ratio, and total contents on the properties of a composite solid propellant. Propellants, Explos. Pyrotech. 45 (9), 1376–1381. https://doi.org/10.1002/prep.202000055.

Polis, M., Szydło, K., Jarosz, T., Procek, M., Skóra, P., Stolarczyk, A., 2022. Investigation of combustion of KMnO4/Zn pyrotechnic delay composition. Mater 15 (18), 6406. https://doi.org/10.2514/1.B37279.

Rao, D.C.K., Yadav, N., Joshi, P.C., 2016. Cu–Co–O nano-catalysts as a burn rate modifier for composite solid propellants. Def. Technol. 12 (4), 297–304. https://doi.org/10.1016/j.dt.2016.01.001.

Schuch, D., Fisch, G., 2019. Rocket emissions representation in atmospheric air-quality models: the short-range atmospheric transport and reaction of gases released by solid propellant engines. Meteorol. Appl. 26 (2), 171–181. https://doi.org/10.1002/met.1750.

Shi, F.J., Feng, S.J., 2024. Oxidation effectiveness and kinetics of potassium permanganate on low-permeability phenanthrene-contaminated soil under fracturing conditions. Chem. Eng. J., 154373 https://doi.org/10.1016/j.cej.2024.154373.

Sun, W., Guo, S., Liu, Y., Sun, Z., Cheng, W., Wei, X., Cao, Y., 2022. The desulfurization of coal tar pitch with potassium permanganate oxidation method. Fuel 323, 124230. https://doi.org/10.1016/j.fuel.2022.124230.

Terry, B.C., Sippel, T.R., Pfeil, M.A., Gunduz, I.E., Son, S.F., 2016. Removing hydrochloric acid exhaust products from high-performance solid rocket propellant using aluminium-lithium alloy. J. Hazard. Mater. 317, 259–266. https://doi.org/10.1016/j.jhazmat.2016.05.067.

Trache, D., Klapötke, T.M., Maiz, L., Abd-Elghany, M., DeLuca, L.T., 2017a. Recent advances in new oxidisers for solid rocket propulsion. Green Chem. 19 (20), 4711–4736. https://doi.org/10.1039/C7GC01928A.

Trache, D., Klapötke, T.M., Maiz, L., Abd-Elghany, M., DeLuca, L.T., 2017b. Recent advances in new oxidisers for solid rocket propulsion. Green Chem. 19 (20), 4711–4736. https://doi.org/10.1039/C7GC01928A.

Trache, D., Maggi, F., Palmucci, I., DeLuca, L.T., 2018. Thermal behavior and decomposition kinetics of composite solid propellants in the presence of amide burning rate suppressants. J. Therm. Anal. Calorim. 132, 1601–1615. https://doi.org/10.1007/s10973-018-7160-8.

Vellaisamy, U., Biswas, S., 2020. Effect of metal additives on neutralization and characteristics of AP/HTPB solid propellants. Combust. Flame 221, 326–337. https://doi.org/10.1016/j.combustflame.2020.08.006.

Wang, S., Ye, B., An, C., Wang, J., Li, Q., 2019. Synergistic effects between Cu metal–organic framework (Cu-MOF) and carbon nanomaterials for the catalyzation of the thermal decomposition of ammonium perchlorate (AP). J. Mater. Sci. 54 (6), 4928–4941. https://doi.org/10.1007/s10853-018-03219-4.

Xiong, W., Liu, Y., Zhang, T., Wu, S., Zeng, D., Guo, X., Pang, A., 2023. Effect of Al–Li alloy on the combustion performance of AP/RDX/Al/HTPB propellant. Aerospace 10 (3), 222. https://doi.org/10.3390/aerospace10030222.

Xu, P., Liu, J., Zhang, L., Yuan, J., Song, M., Liu, H., 2021. Composition of solid and gaseous primary combustion products of boron-based fuel-rich propellant. Acta Astronaut. 188, 36–48. https://doi.org/10.1016/j.actaastro.2021.07.006.

Yang, L., Mi, Z., Fang, H., Xu, R., Lv, B., Li, J., Zhang, G., 2024. Fabrication of highly catalytic active α-Fe_2O_3-carbon Nanotube composites for thermal decomposition of ammonium perchlorate by light and temperature control strategy. Surf. Interfaces 44, 103642. https://doi.org/10.1016/j.surfin.2023.103642.

Yildiz, M. S., Kokal, U., and Celik, M. "Preliminary Thrust Measurement Results of the BUSTLab Microwave Electrothermal Thruster." In 53rd AIAA/SAE/ASEE Joint Propulsion Conference, p. 4725. https://doi.org/10.2514/6.2017-4725.

Yuan, J., Liu, J., Zhou, Y., Zhang, Y., Cen, K., 2021. Thermal decomposition and combustion characteristics of Al/AP/HTPB propellant. J. Therm. Anal. Calorim. 143, 3935–3944. https://doi.org/10.1007/s10973-020-09297-4.

Zhang, Y., Zhao, Z., Xing, D., Hu, J., Liu, W., Wang, X., Yao, L., 2024. Effect of inorganic salts/lignin on the combustion performance of torrefied biochar. Energy 293, 130707. https://doi.org/10.1016/j.energy.2024.130707.